Biosensors and Bioelectronics 133 (2019) 16–23

Contents lists available at ScienceDirect

Biosensors and Bioelectronics

journal homepage: www.elsevier.com/locate/bios

Biophysical phenotyping of single cells using a differential multiconstriction microfluidic device with self-aligned 3D electrodes

Dahou Yang[a,1], Ying Zhou[b,1], Yinning Zhou[a], Jongyoon Han[b,c], Ye Ai[a,*]

[a] Pillar of Engineering Product Development, Singapore University of Technology and Design, Singapore 487372, Singapore
[b] BioSystems and Micromechanics IRG (BioSyM), Singapore-MIT Alliance for Research and Technology (SMART) Centre, Singapore 138602, Singapore
[c] Department of Electrical Engineering and Computer Science, and Department of Biological Engineering, Massachusetts Institute of Technology, Cambridge, MA 02139, USA

ARTICLE INFO

Keywords:
Biophysical cellular biomarker
Cell deformability
Electrical impedance spectroscopy
Microfluidic cytometry
Single cell analysis

ABSTRACT

Precise measurement of mechanical and electrical properties of single cells can yield useful information on the physiological and pathological state of cells. In this work, we develop a differential multiconstriction microfluidic device with self-aligned 3D electrodes to simultaneously characterize the deformability, electrical impedance and relaxation index of single cells at a high throughput manner (> 430 cell/min). Cells are pressure-driven to flow through a series of sequential microfluidic constrictions, during which deformability, electrical impedance and relaxation index of single cells are extracted simultaneously from impedance spectroscopy measurements. Mechanical and electrical phenotyping of untreated, Cytochalasin B treated and N-Ethylmaleimide treated MCF-7 breast cancer cells demonstrate the ability of our system to distinguish different cell populations purely based on these biophysical properties. In addition, we quantify the classification of different cell types using a back propagation neural network. The trained neural network yields the classification accuracy of 87.8% (electrical impedance), 70.1% (deformability), 42.7% (relaxation index) and 93.3% (combination of electrical impedance, deformability and relaxation index) with high sensitivity (93.3%) and specificity (93.3%) for the test group. Furthermore, we have demonstrated the cell classification of a cell mixture using the presented biophysical phenotyping technique with the trained neural network, which is in quantitative agreement with the flow cytometric analysis using fluorescent labels. The developed concurrent electrical and mechanical phenotyping provide great potential for high-throughput and label-free single cell analysis.

1. Introduction

Cellular biophysical properties (e.g., mechanical and electrical properties) are promising label-free biomarkers for classifying different cell types and studying their developmental stages (Chen et al., 2011; Kim et al., 2018; Teng et al., 2018; Zhou et al., 2018). It has been proved that changes in cell deformability are related to several diseases such as cancer (Byun et al., 2013; Teng et al., 2017), sepsis (Donadello et al., 2015), and diabetes (Agrawal et al., 2016). For example, red blood cells infected with malaria parasites are much stiffer than normal red blood cells (Guo et al., 2012; Yang et al., 2017). Standard tools for studying the mechanical properties of single cells include atomic force microscopy (Haase and Pelling, 2015), micropipette (Hochmuth, 2000), and optical stretching (Ekpenyong et al., 2017). However, the throughput of these techniques is usually very low (< 1 cell/min), in addition the operation is labor-intensive and time-consuming.

Recently, microfluidics-based technologies, for example hydrodynamic stretching-based techniques (Gossett et al., 2012) and constriction-based methods (Apichitsopa et al., 2018; Dylan Tsai et al., 2014), have been developed to characterize cell deformability at single cell level. High-speed camera setups are usually employed to visually capture the motion and shape change of single cells, and then the cell deformability is quantified by evaluating the elongation and compression of a single cell compared with its original circularity (hydrodynamic stretching), or the transit time of a cell passing through a constriction channel (constriction-based techniques). However, the high-speed camera setup is expensive, and also generates a huge amount of useless images without cell events that require an intricate image-processing algorithm to extract useful information. On the other hand, the integration of electrical impedance measurement with constriction-based technique, eliminating the use of high-speed cameras, serves as a promising alternative approach for accurately measuring the

* Corresponding author.
E-mail address: aiye@sutd.edu.sg (Y. Ai).
[1] These authors contributed equally to this work.

https://doi.org/10.1016/j.bios.2019.03.002
Received 1 December 2018; Received in revised form 1 March 2019; Accepted 1 March 2019
Available online 07 March 2019
0956-5663/

transit time of a single cell passing through a microfluidic constriction (Adamo et al., 2012). A common configuration of such devices is that two electrodes are placed on either side of a single constriction (Adamo et al., 2012; Yang et al., 2017). An AC voltage is applied to one electrode and the electrical current is measured from the other electrode. When a single cell flows through the constriction, it temporally blocks the electrical fields inside the constriction, giving rise to an increase in electrical impedance across the two electrodes. The transit time of a single cell through the constriction is calculated by extracting the time duration between the impedance changes at the entrance and exit, and it can be used as an indicator of cell deformability. This technique provides advantages such as high throughput and simple data processing for rapid, real-time analysis of single cells. Furthermore, this technique not only enables the assessment of cellular mechanical properties but also provides information on cellular electrical properties (Chen et al., 2011; Zheng et al., 2012; Zhou et al., 2018). The electrical impedance of single cells, which are mainly determined by the electrical properties of cell membrane and cytoplasm, can also be used as label-free biomarkers for single cell analysis, such as stem cell differentiation (Zhou et al., 2016a), cell phenotype (Huang et al., 2018; Zhao et al., 2013), and leukocyte activation (Petchakup et al., 2018).

Existing microfluidic devices for electrical impedance measurement usually consist of a PDMS layer containing microfluidic channels and an electrode substrate (Zhou et al., 2016a). The fabrication of the electrode substrate involves multiple steps, including photolithography, metal deposition and lift-off. These electrode fabrication steps often require complex and sophisticated equipment (e.g., e-beam evaporator or sputtering machine for metal deposition), which is generally expensive, relatively slow and not readily accessible. In addition, the bonding of electrode patterns and PDMS channels also requires precise alignment, making this process challenging and time-consuming (Ma et al., 2016). Compared with conventional microfabricated coplanar electrodes, the use of low melting point alloys provides a much simpler approach to fabricate self-aligned 3D electrodes and also generate uniform 3D electric fields (Herling et al., 2013; Puttaswamy et al., 2015; So and Dickey, 2011). The low melting point alloy (e.g., In/Bi and/Sn alloy) has a melting point of a certain temperature (e.g., 60 °C), meaning that it is essentially a 'liquid electrode' above that temperature, but a solid electrode at room temperature. In other words, the low melting point alloy can flow into the electrode channel as a liquid at a certain temperature during fabrication to form 3D electrodes. At room temperature, the 3D electrodes solidify and can be used as solid impedance sensing electrodes, which are not susceptible to surrounding environments such as pressure.

Current impedance-based deformability characterization devices usually employ the single-constriction channel to let single cells pass through and then characterize their deformability and electrical impedance (Adamo et al., 2012; Chen et al., 2011). For example, in our previous work (Zhou et al., 2018), a single-constriction microfluidic device was developed to simultaneously measure the mechanical and electrical properties of single cells. Most recently, multiconstriction microfluidic devices have been demonstrated to study the cell deformation and relaxation behaviour (Gabriele et al., 2009; Mak and Erickson, 2013) and improve the efficacy in distinguishing cancer cell from normal cells compared with the single-constriction channel device (Ren et al., 2018). Cell relaxation after deformation plays an important role in the cellular migration such as microcirculation of red blood cells in the capillaries of blood vessels (Braunmüller et al., 2012) and cancer metastasis (Wirtz et al., 2011), as well as acting as a protective mechanism against mechanical damage (Bonakdar et al., 2016). However, existing multiconstriction microfluidic device capable of evaluating the cellular relaxation properties (e.g., relaxation time (Braunmüller et al., 2012)) heavily relies on the high-speed imaging capability.

In this work, we have developed a differential multiconstriction microfluidic device with self-aligned 3D electrodes using low melt point alloy to simultaneously measure the deformability, electrical impedance and relaxation index of MCF-7 breast cancer cells, i.e., biophysical phenotyping at single cell level. The total transit time and average electrical impedance of single cells passing through the multiconstriction channels were studied and used as the indicators for cell

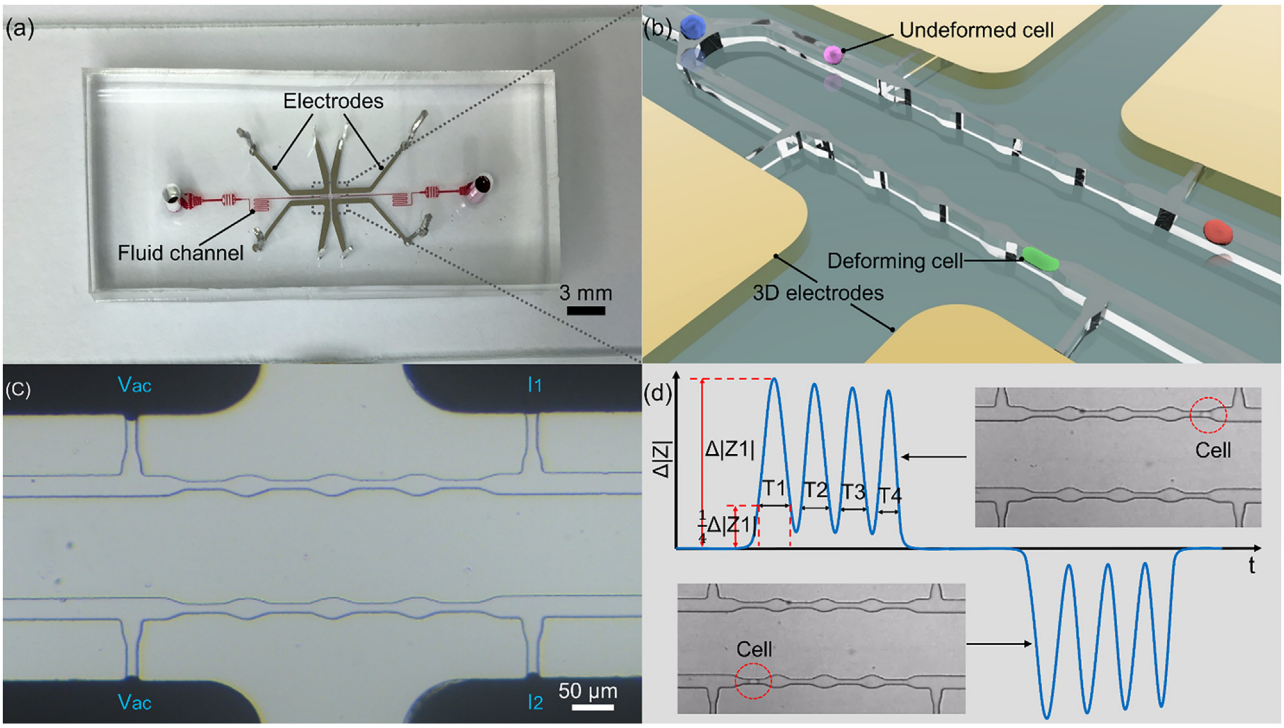

Fig. 1. Overview, structure and working principle of our microfluidic biophysical phenotyping device. (a) An image of the fabricated device filled with red dye. (b) An enlarged 3D schematic of the constriction area (transparent color) with self-aligned electrodes (golden color) and flowing cells. (c) A microscopic image of the constriction area, with notations illustrating the setup of electrical measurement. (d) Schematic diagram showing the working principle and resulting signal profile.

deformability and electrical properties, respectively. A differential multiconstriction channel was designed to investigate the cell deformation and relaxation process based on the electrical impedance measurement instead of using image analysis, which cannot be achieved by the conventional impedance-based deformability flow cytometry with single-constriction channels. Relaxation index of single cells was investigated by comparing the transit time information of cells through successive constrictions. Furthermore, a back propagation neural network was developed and applied to quantify the cell type classification based on the three measured biophysical properties. Results demonstrated that biophysical phenotyping with the three properties together can significantly improve the classification accuracy with high sensitivity and specificity, providing great potential for single cell detection and classification.

2. Material and methods

2.1. Working principle and device design

An overview of the fabricated microfluidic device filled with a red dye for better visualization is illustrated in Fig. 1a. Fig. 1b shows the 3D schematic of the constriction area as well as the electrode (golden color). There are two identical flow pathways for individual cells to flow through, and both pathways consist of four successive constrictions (50 μm in length, 10 μm in width and 20 μm in height) and three relaxation regions (50 μm in length, 25 μm in width and 20 μm in height). These channel dimensions were designed to fit the size of MCF-7 breast cancer cells used in the experiments.

In this microfluidic biophysical phenotyping device, 3D electrodes are self-aligned and in direct contact with the fluidic channels for electrical impedance measurement. A differential electrical impedance measurement can be utilized in the experiments because of the differential channel design. As shown in Fig. 1c, where a microscopic image of the constriction area is presented, an input voltage V_{ac} (50 kHz; 2 V) is applied to the two left electrodes, and currents are measured from the upper right (I_1) and lower right (I_2) electrodes to calculate the differential impedance ($\Delta|Z|$). As shown in Fig. 1d, when a cell passes through the upper pathway, the impedance of the single cell is measured by the upper two electrodes; while the lower two electrodes measure the electrical impedance of the medium. The lower two electrodes in return work as the sensing electrodes to measure the cell impedance when a cell passes through the lower pathway. When a single cell squeezes into the constriction, the less conductive cell blocks the electrical field lines in the constriction, thereby leading to an increase in the electrical impedance. Due to the employment of differential impedance measurement scheme, there will be four sequential impedance peaks above the signal baseline (i.e., positive peaks) as a cell passes through the four constrictions in the upper pathway, and there will be four sequential impedance peaks below the signal baseline (i.e., negative peaks) when a cell passes through the lower pathway. The differential impedance measurement can cancel out any common mode drifts caused by the electrode properties or surrounding environment changes such as the temperature and conductivity (Gawad et al., 2001; Zhou et al., 2016b). The transit time of a cell squeezing through each constriction can be determined, based on the width of each impedance peak at the 1/4 peak height. T1, T2, T3 and T4 represent, respectively, the transit time of the cell passing through the first, second, third and fourth constrictions, and corresponding differential impedance magnitudes are notated as $\Delta|Z1|$, $\Delta|Z2|$, $\Delta|Z3|$ and $\Delta|Z4|$, respectively. For a given cell size, its transit time mainly reflects the cell deformability and the magnitude of each impedance peak is dependent on the electrical properties of cells.

The deformed cell will relax back to its initial shape after released from the constriction. In order to evaluate the cell deformation and relaxation process through the successive constrictions, the transit time of the cell through the last constriction (T4) and the first constriction (T1) are compared. The ratio of T4 to T1 is calculated and defined as relaxation index (i.e., relaxation index = T4/T1), serving as an indicator of the cell relaxation capacity. Consider two extreme cases: the case where a cell relaxes very fast and the case where the cell relaxes very slowly. If a cell relaxes very fast (i.e., shorter than the time required to pass through the relaxation region), the cell would recover to nearly a spherical shape before entering the next constriction. Therefore, the cell enters each constriction with a nearly consistent shape and mechanical property. As a result, the time required for the cell to transit through the last constriction should be comparable with the time for the cell transiting through the first constriction. In this case, the relaxation index will be close to unity. On the contrary, if a cell relaxes very slowly, it would retain a deformed shape before entering the last constriction, and thus requires less time to transit through that constriction, compared with the time required to transit through the first constriction. In this case, the relaxation index would be remarkably smaller than unity.

A finite element simulation using COMSOL in Fig. S1 shows the electrical field strength distribution inside the constriction channels in the presence and absence of a single cell. Video S1 demonstrates the electrode fabrication process and Fig. S2 shows a finalized device. Details of the electrical field simulation and device fabrication are presented in Supplementary Information.

Supplementary material related to this article can be found online at doi:10.1016/j.bios.2019.03.002.

2.2. Cell preparation

To ensure consistency, MCF-7 breast cancer cells from the same lot were cultured in standard conditions using the medium from the same lot. Cytochalasin B-treated MCF-7 (i.e., CB-MCF-7) and N-Ethylmaleimide-treated MCF-7 (i.e., NEM-MCF-7) were prepared by incubating MCF-7 in 150 μM CB (Cytochalasin B) and 1 mM NEM (N-Ethylmaleimide) at 37 °C for one hour, respectively. After the treatments, cells were spun down and resuspended in PBS for measurements. The three cell populations used in this work were found to be in a similar size range (13–22 μm) (Fig. S3) and separately measured by our device. In order to further test the performance of our microfluidic system, MCF-7 and NEM-MCF-7 cells were mixed together and then divided into two sample groups. Since NEM-MCF-7 cells were dead after the treatment of 1 mM NEM, propidium iodide (PI) solution (1.0 mg/ml in water) was used to stain the first sample to distinguish the MCF-7 and NEM-MCF-7 cells using flow cytometry (MACSQuant Analyzer). The nuclei staining dye PI cannot pass through a live cell membrane and therefore only NEM-MCF-7 cells were stained. The second sample was measured in our microfluidic device without staining for the comparison with flow cytometry.

2.3. Experimental setup and data analysis

The fluidic flow in the microfluidic device was controlled by a pressure control system (Fluigent MFCS-EZ). A positive pressure was applied at the fluidic inlet of the device to drive the flow. Generally, a high fluid driving pressure results in a high throughput, at a price of sacrificing the time resolution during the transit time measurement. Here, we select 500 mbar as the fluid driving pressure to balance the throughput and sensitivity. Before the cells were injected into the microchannel, microfluidic channels were filled with 1% BSA (in PBS) for 20 min to prevent any non-specific adsorption of cells to the channel walls (Hou et al., 2009). Cells were then continuously introduced into the device at the desired pressure. Electrical impedance data were recorded by an impedance spectroscope (HF2IS, Zurich Instruments) and analysed using a custom-written Matlab program (MATLAB, Mathworks, USA).

In order to evaluate the efficiency of the classification of different cell types based on the concurrent mechanical and electrical

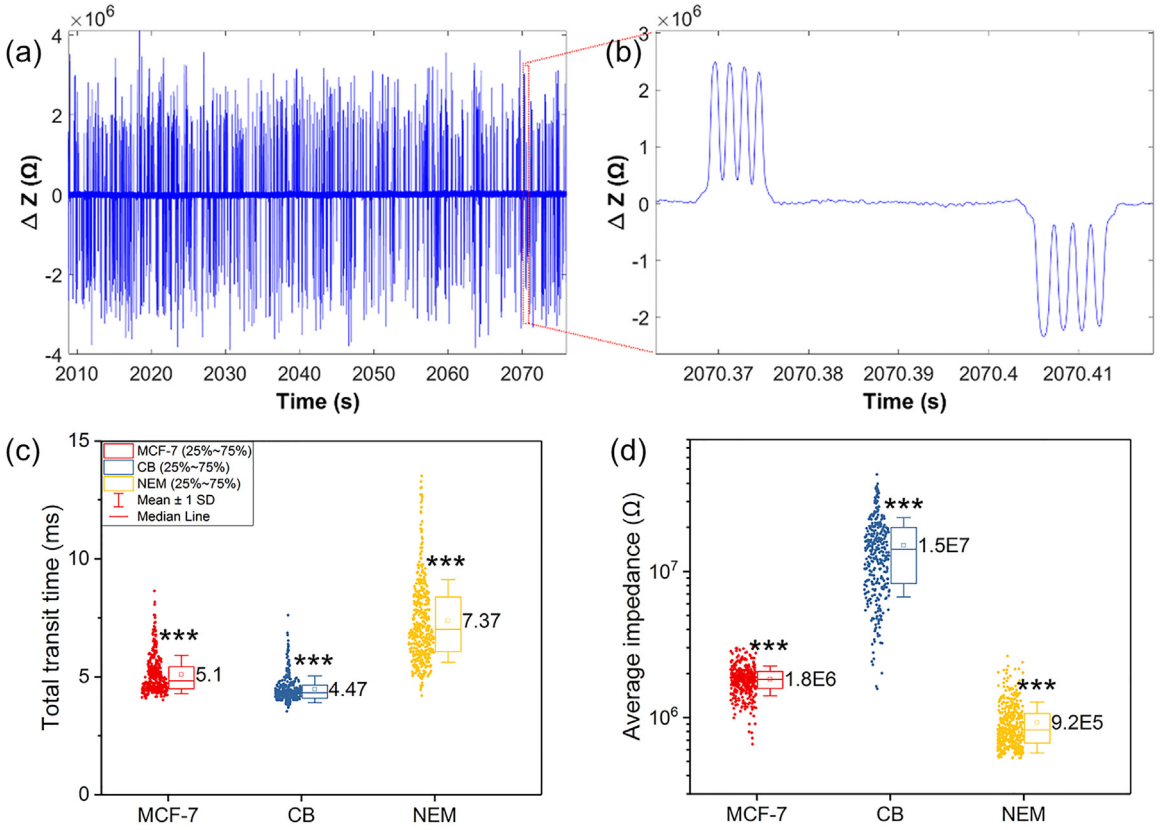

Fig. 2. Examples of the measured impedance signal, total transit time and average impedance extracted from the signal. (a) Impedance signal of MCF-7 cells measured at 50 kHz frequency and 500 mbar flow pressure. (b) An enlarged view of the impedance signal, demonstrating the event where one cell transits through the upper pathway followed by another cell passing through the lower pathway. (c) Total transit time and (d) average electrical impedance of cells passing through four successive constrictions for three cell populations. Cell numbers of MCF-7, CB-MCF-7 and NEM-MCF-7 are: 336, 330 and 428. The numbers near the box charts indicate the mean values of total transit time or electrical impedance. *** means there is a significant difference among cell populations ($p < 0.001$), based on the Mann – Whitney test.

phenotyping, a back propagation neural network (Pedregosa et al., 2011; Rashid, 2016) (Python 3.5) consisting of three layers was used for pattern recognition. The whole dataset is divided into three parts, including training data (70%), validation data (15%) and test data (15%), to quantify the cell classification accuracy (true classification/total population). The principle of used back propagation neural network is illustrated in Fig. S4 and presented in Supplementary Information.

3. Results and discussion

The functionality of the fabricated microfluidic device was validated by characterizing the three biophysical properties of chemically treated MCF-7 cells and normal MCF-7 cells, which are commonly used in the cell deformability study (Wu et al., 2018). Fig. 2a exemplifies the impedance signal of MCF-7 cells passing through the constriction regions, measured from one single experiment. As shown in Fig. 2b, where an enlarged view of the impedance signal is presented, as a single cell transits through the upper pathway, four successive impedance peaks are observed, respectively corresponding to the moments when the cell passes through the four constrictions in the upper pathway. Similarly, four impedance peaks are generated when a single cell transits through the lower pathway. It can be observed that the peak width and magnitude decrease as cells pass through successive constrictions and undergo repeated deformation. Video S2 shows the similar cases where a cell passes through the lower pathway followed by a cell passing through the upper pathways. The throughput is more than 430 cells/min in this experiment, which can be further improved by using higher driving pressure to increase the flow rate, or by optimizing cell concentrations.

Supplementary material related to this article can be found online at doi:10.1016/j.bios.2019.03.002.

3.1. Deformability and electrical impedance study

To verify that the transit time of cells passing through a constriction is determined by the deformability of cells, three populations of cells (normal MCF-7, CB-treated MCF-7 and NEM-treated MCF-7) were investigated using the microfluidic device. Cytochalasin B (CB) is a microfilament-disrupting agent, which has been reported to increase cell deformability (Adamo et al., 2012; Mazur, 1977). N-ethylmaleimide (NEM) is a sulfhydryl-binding agent and has been found to reduce cell deformability (Mazur, 1977). As shown in Fig. S3, the three populations of cells tested in this work exhibit similar cell size distributions. Since the transit time of single cells is also influenced by the cell size (Adamo et al., 2012; Zhou et al., 2018) the same cell size distributions here ensure that the transit time is primarily dependent on the cell deformability rather than the cell size. Fig. 2c illustrates the total transit time (total transit time = T1 + T2 + T3 + T4) for cells to pass through the four constrictions. NEM-MCF-7 cells show the longest total transit time (7.4 ± 1.8 ms) due to the NEM treating, while CB-MCF-7 cells exhibit the shortest total transit time (4.5 ± 0.6 ms) because of the CB treating. Based on the total transit time information, it can be inferred that the NEM-MCF-7 cells are the least deformable one as these cells require the longest time to pass through constriction regions. On the contrary, CB-treated MCF-7 cells are the most deformable one. The deformability of normal MCF-7 cells sits in between NEM-treated and CB-treated MCF-7 cells. This result agrees with the findings in the literature that NEM makes cells less deformable and CB makes the cells

more deformable (Adamo et al., 2012; Mazur, 1977). The total transit time among these three cell populations shows statistical significance ($p < 0.001$), based on the Mann – Whitney test.

Fig. 2d presents the average impedance magnitude of the four sub-peaks (i.e., $\Delta Z_{average} = (\Delta Z1 + \Delta Z2 + \Delta Z3 + \Delta Z4)/4$) for all the three populations, measured at 50 kHz frequency. As an individual cell squeezes into the constriction, the cross-section of the constriction is mostly blocked by the deformed cell. In this case, the total electrical current is composed of the current through the cell membrane and intracellular contents, and the leakage current through the gap between the cell surface and channel wall. For the same cell type, to some extent, a larger cell means a smaller gap and thus larger impedance magnitude. Since the three cell populations tested here have a similar size (Fig. S3), the difference in their electrical impedance is mainly determined by the difference in the electrical properties of cell membranes and intracellular structures. NEM-MCF-7 cells were dead after the NEM treatment and their membranes were no longer a barrier to electrical current, meaning that the equivalent electrical conductance of cells increased after they were treated with NEM. Therefore, NEM-MCF-7 cells exhibit the lowest impedance magnitude. On the other hand, CB-MCF-7 cells present the largest impedance magnitude, which might be caused by the change in electrical properties of the cell membrane. The capacitance of the cell membrane seemed to have decreased after CB treatment, which led to an increase in the impedance magnitude, compared with the untreated MCF-7 cells. The untreated MCF-7 cells serve as the control group and their impedance magnitude resides in between NEM-treated and CB-treated MCF-7 cells. Since the size of these three cell populations is in a similar range, they cannot be easily discriminated or separated by size-based techniques such as inertial sorting (Hou et al., 2013). However, based on the characterization of their electrical properties, these three cell populations show a significant difference among them ($p < 0.001$ based on the Mann – Whitney test).

3.2. Cell deformation and relaxation through successive constrictions

For the transit time through individual constrictions, as shown in Fig. 3, it is found that the transit time for a single cell to pass through the first constriction is generally longer than the time it needs to pass through the second, third or fourth constriction. This is because the pre-deformation facilitates the cell transit through the subsequent constrictions. Detailed discussions of the transit time and electrical impedance (Fig. S5) through individual constrictions are presented in the Supplementary Information.

As discussed in the working principle section, the ratio of T4 to T1 is defined to evaluate the cell deformation and relaxation process (i.e., relaxation index = T4/T1). A value of relaxation index closer to the unity means the cell relaxes faster, and vice versa. As shown in Fig. 4a, a significant difference in the relaxation index has been observed among all the three cell populations ($p < 0.001$). CB-MCF-7 cells have the highest relaxation index (0.95 ± 0.06), meaning that these cells relax the fastest among the three cell populations. NEM-MCF-7 cells have the lowest value (0.84 ± 0.11), indicating that these cells relax the slowest. NEM-MCF-7 cells were dead after the NEM treatment and their mechanical properties were changed as indicated by the increased total transit time. It has been reported that incomplete cell relaxation is due to an additive plastic deformation (Bonakdar et al., 2016). The dead NEM-MCF-7 cells may undergo a higher proportion of plastic deformation and thus be more difficult to relax back to its original shape, resulting in the lowest relaxation index. The relaxation index evaluated in this work may serve as a new promising mechanical biomarker for single cell level biophysical phenotyping.

The developed microfluidic device enables the simultaneous characterization of the cell deformability, electrical impedance and relaxation index. These biophysical properties are combined together in this work to achieve a better classification of different cell types. As shown in Fig. 4b, three cell populations can be clearly distinguished from each other, which cannot be accomplished just based on single-domain parameter.

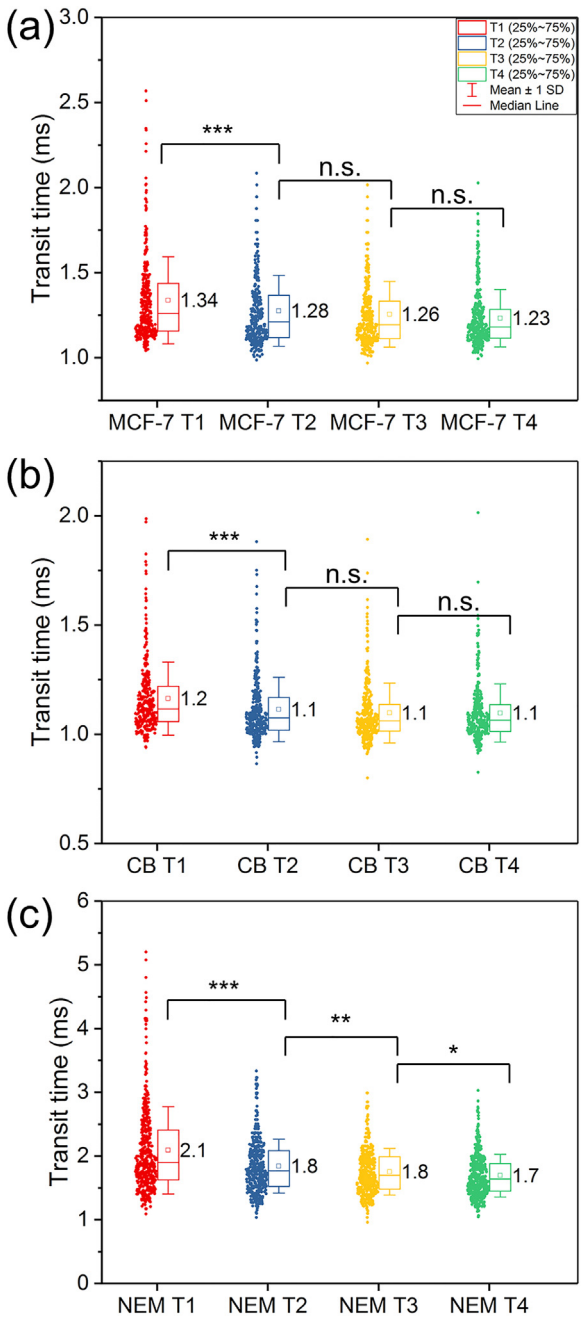

Fig. 3. Transit time of cells passing through each of the four successive constrictions. The transit time is presented for all the three cell populations (MCF-7(a), CB-MCF-7(b) and NEM-MCF-7(c)). Cell numbers of MCF-7, CB-MCF-7 and NEM-MCF-7 are: 336, 330 and 428. The numbers near the box charts indicate the mean values of time. ***, **, * and n.s. indicate a p-value of less than 0.001, 0.01, 0.05 and larger than 0.05 (statistically nonsignificant), respectively, based on the Mann-Whitney test.

3.3. Classification of cell types based on neural network

With the three measured biophysical properties as the inputs for the aforementioned propagation neural network, we quantitatively evaluate their efficiency for the cell type classification. The trained neural network achieved the classification accuracy of 87.8% (electrical

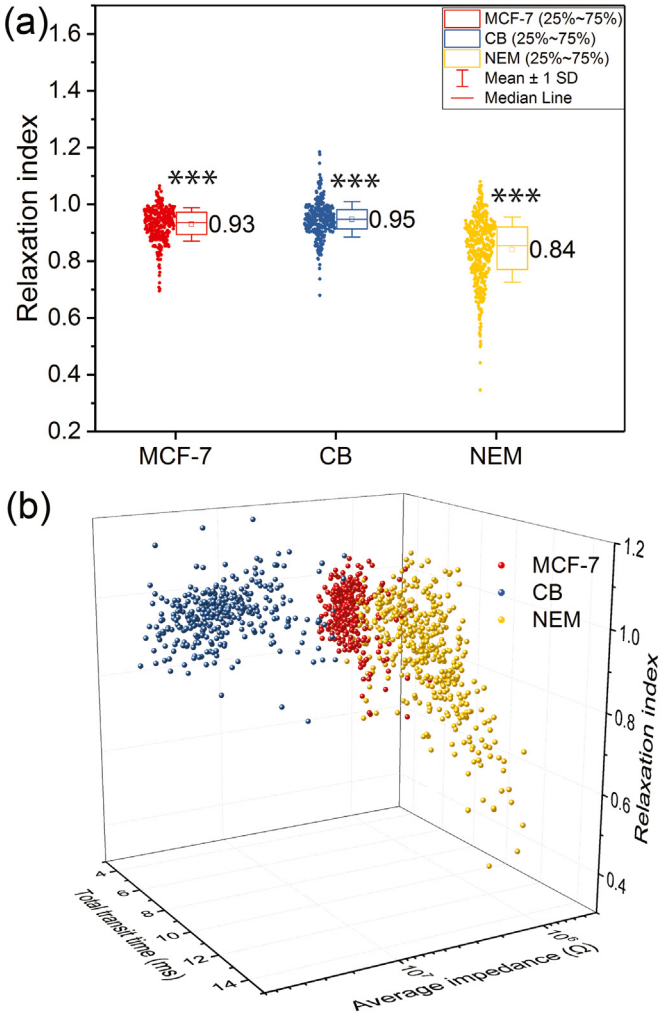

Fig. 4. Relaxation index and the 3D scatterplot of electrical impedance vs total transit time vs relaxation index. (a) Relaxation index, namely, the ratio of the transit time of a single cell transiting through the fourth constriction to the transit time of the cell transiting through the first constriction. (b) Different cell populations can be clearly distinguished by combing the three biophysical properties (i.e., electrical impedance, total transit time and relaxation index). Cell numbers of MCF-7, CB-MCF-7 and NEM-MCF-7 are: 336, 330 and 428. The numbers near the box charts indicate the mean values of time. *** indicates that there is a significant difference among cell populations ($p < 0.001$), based on the Mann – Whitney test.

impedance), 70.1% (total transit time), 42.7% (relaxation index) and 93.3% (combination of electrical impedance, total transit time and relaxation index) for the test group. Besides the classification accuracy of 93.3% (true classification/total population), the average sensitivity (true positive/(true positive + false negative)) of 93.3% and specificity (true negative/(true negative + false positive)) of 93.3% for the test group were also achieved. Fig. 5 illustrates the confusion matrix that contains information regarding the true and predicted classifications, which are presented by the neural network. As shown in Fig. 5a, there are more confusions between MCF-7 and NEM-MCF-7. For example, in the training confusion matrix, there are 28 MCF-7 cells misclassified as NEM-MCF-7 and 12 NEM-MCF-7 cells misclassified as MCF-7. However, only 8 MCF-7 cells are misidentified as CB-MCF-7 and 3 CB-MCF-7 cells are misidentified as MCF-7. This is due to the appearance of more overlaps in the electrical impedance and mechanical properties (i.e., total transit time and relaxation index) between MCF-7 and NEM-MCF-7 cells, which can be observed from Fig. 2c, Figs. 2d and 4a. Since the number of each cell type is not equal, confusion matrix with normalization was performed to have a more visual interpretation of which cell population is misclassified. As shown in Fig. 5b, 88% percent of MCF-7, 98% percent of NEM-MCF-7% and 94% percent of NEM-MCF-7 are correctly classified for the test group. The classification accuracy, average sensitivity and specificity for the training and validation group all were higher than 93%, which were listed in Tables S1 and S2.

The mixtures of MCF-7 and NEM-MCF-7 cells were measured using flow cytometry and our device to further verify the performance of this biophysical phenotyping technique. As shown in Fig. 6a, using flow cytometry method, the proportion of MCF-7 and NEM-MCF-7 cells is 23.8% and 70.7%, respectively. Fig. 6b and c show the predicted results presenting by the trained neural network using three parameters as inputs but illustrated as 2D and 3D scatterplot respectively. These biophysical phenotyping results of MCF-7 cells at 22.1% and NEM-MCF-7 cells at 77.9% are comparable to the flow cytometric analysis. And fluorescent labeling process is not needed in the microfluidic biophysical phenotyping technique as compared to flow cytometry.

4. Conclusions

In this work, a differential multiconstriction microfluidic device with 3D electrodes was developed for high-throughput biophysical phenotyping at single cell level, referring to the simultaneous characterization of deformability (i.e., total transit time), electrical impedance and relaxation index of single cells. Compared with previously reported impedance-based microfluidic device for the measurement of electrical and mechanical properties of single cells, the employment of multiconstriction channels instead of single constriction enables the evaluation of relaxation index of single cells and the method developed for the creation of self-aligned 3D electrodes greatly reduces the complexity of device fabrication. The differential electrical impedance strategy was used to cancel out the environmental changes and thus improve the signal-to-noise ratio. The electrical and mechanical phenotyping of normal MCF-7 and chemical-modified MCF-7 cells were investigated in this work and showed significant differences among them. Our developed neural network quantitatively demonstrated that the combination of all the three biophysical properties of single cells can significantly improve the classification accuracy (93.3%) of different cell populations with high sensitivity and specificity. Cell classification of a cell mixture using the trained neural network has achieved quantitative accuracy as compared to conventional flow cytometry. This impedance-based microfluidic device provides great potential for high-throughput and label-free biophysical phenotyping of single cells and thus may be used as a diagnostic tool for some diseases associated with cell mechanical or electrical properties changes. Furthermore, the simple processing of electrical signals enables real-time cell detection, further facilitating downstream cell sorting and separating processes.

CRediT authorship contribution statement

Dahou Yang: Data curation, Formal analysis, Investigation, Methodology, Software, Validation, Visualization, Writing - original draft. **Ying Zhou:** Data curation, Formal analysis, Investigation, Methodology, Software, Validation, Visualization, Writing - original draft. **Yinning Zhou:** Methodology, Resources. **Jongyoon Han:** Conceptualization, Funding acquisition, Investigation, Project administration, Supervision, Writing - review & editing. **Ye Ai:** Conceptualization, Funding acquisition, Investigation, Methodology, Project administration, Resources, Software, Supervision, Writing - review & editing.

Acknowledgements

This work was supported by the Singapore – MIT Alliance for

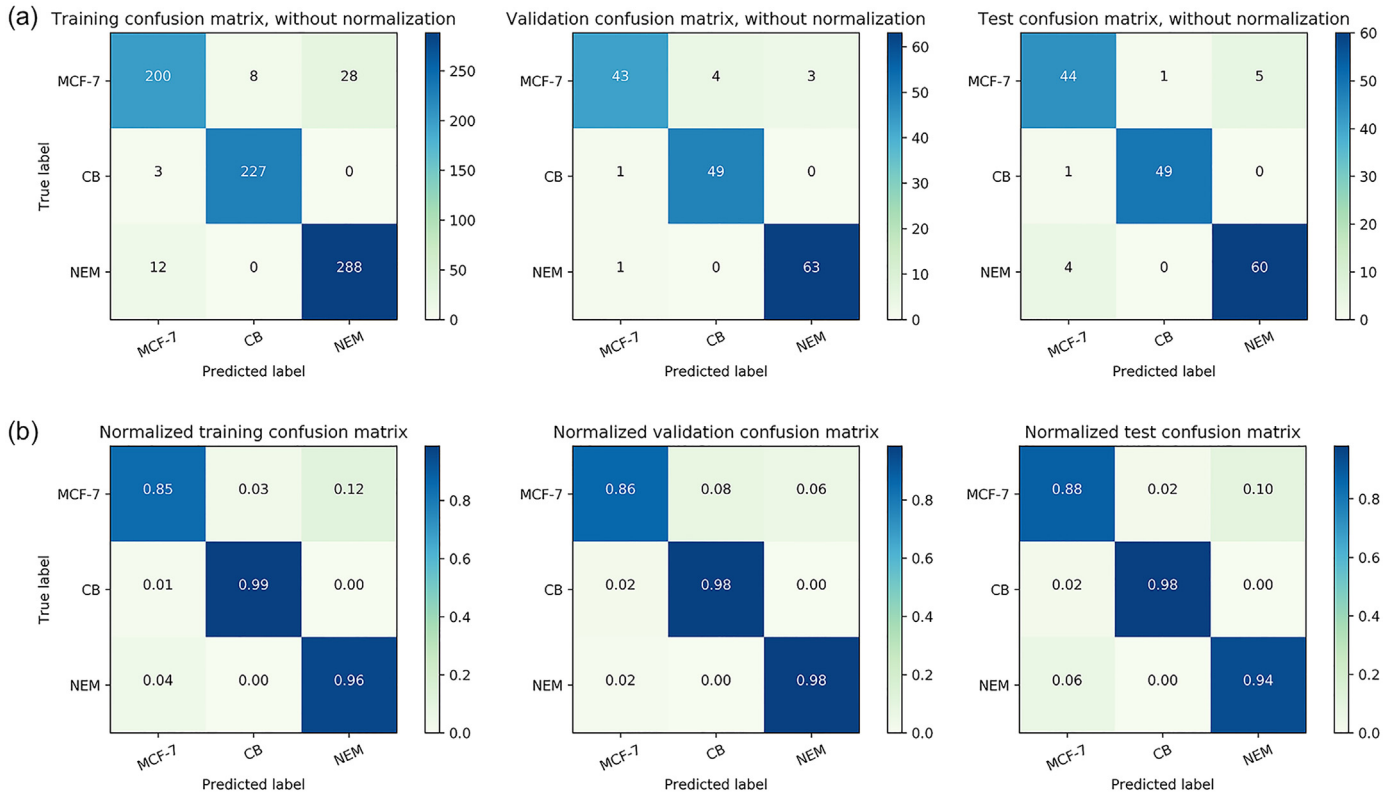

Fig. 5. Confusion matrix illustrating the efficiency of cell type classification using electrical impedance, total transit time and relaxation index. (a) Confusion matrix of the training, validation and test group without normalization. Values on the diagonal represent the number of cells correctly classified, while off-diagonal values represent those incorrectly classified. (b) Confusion matrix of the training, validation and test group with normalization to have a more visual interpretation of which cell population is misclassified. There are more confusions between MCF-7 and NEM-MCF-7 as they have more overlaps in the measured electrical and mechanical properties.

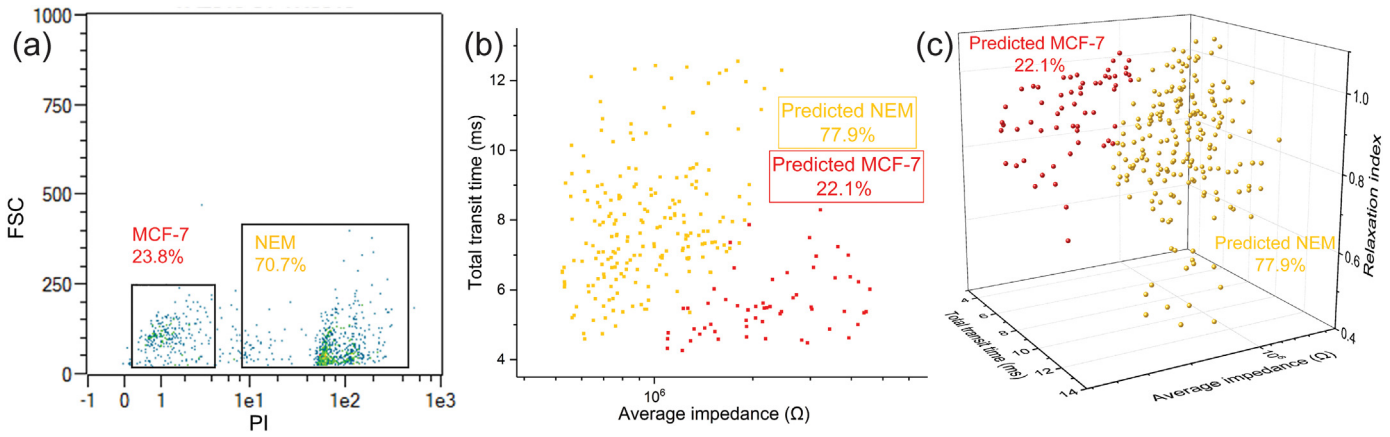

Fig. 6. Cell characterization using flow cytometry and our microfluidic biophysical phenotyping device. (a) Flow cytometric scatter plot of the mixed MCF-7 and NEM-MCF-7 cells. (b) 2D scatter plot and (c) 3D scatter plot of the mixed MCF-7 and NEM-MCF-7 cells using the trained neural network with electrical impedance, total transit time and relaxation index as inputs.

Research and Technology (SMART) Centre, BioSystems and Micromechanics (BioSyM) IRG, which was funded by the National Research Foundation (NRF) of Singapore, and also in part supported by Singapore Ministry of Education – Singapore Academic Research Fund Tier 2 (T2MOE1603). D.Y. gratefully acknowledges the President's Graduate Fellowship awarded by the Ministry of Education (MOE), Singapore. Y.Z. is supported by a seed grant from BioSyM IRG.

Credit author statement

Y.A. and J.H. conceived of the presented idea. D.Y. and Y.Z. fabricated the microfluidic devices, built the experimental set-up, performed the experiments, and wrote the manuscript. D.Y. and Y.A. developed the neural network. Y.N.Z. prepared the tested biological samples. Y.A. and J.H. helped the experimental design, analyzed the data, interpreted the results, and revised the manuscript. All authors read and approved the completed manuscript.

Declaration of interests

None.

Conflicts of interest

The authors declare no conflict of interest.

Appendix A. Supplementary material

Supplementary data associated with this article can be found in the online version at doi:10.1016/j.bios.2019.03.002.

References

Adamo, A., Sharei, A., Adamo, L., Lee, B., Mao, S., Jensen, K.F., 2012. Microfluidics-based assessment of cell deformability. Anal. Chem. 84 (15), 6438–6443.

Agrawal, R., Smart, T., Nobre-Cardoso, J., Richards, C., Bhatnagar, R., Tufail, A., Shima, D., Jones, P.H., Pavesio, C., 2016. Assessment of red blood cell deformability in type 2 diabetes mellitus and diabetic retinopathy by dual optical tweezers stretching technique. Sci. Rep. 6, 15873.

Apichitsopa, N., Jaffe, A., Voldman, J., 2018. Multiparameter cell-tracking intrinsic cytometry for single-cell characterization. Lab Chip 18 (10), 1430–1439.

Bonakdar, N., Gerum, R., Kuhn, M., Sporrer, M., Lippert, A., Schneider, W., Aifantis, K.E., Fabry, B., 2016. Mechanical plasticity of cells. Nat. Mater. 15 (10), 1090–1094.

Braunmüller, S., Schmid, L., Sackmann, E., Franke, T., 2012. Hydrodynamic deformation reveals two coupled modes/time scales of red blood cell relaxation. Soft Matter 8 (44), 11240.

Byun, S., Son, S., Amodei, D., Cermak, N., Shaw, J., Kang, J.H., Hecht, V.C., Winslow, M.M., Jacks, T., Mallick, P., 2013. Characterizing deformability and surface friction of cancer cells. Proc. Natl. Acad. Sci. USA 110 (19), 7580–7585.

Chen, J., Zheng, Y., Tan, Q., Shojaei-Baghini, E., Zhang, Y.L., Li, J., Prasad, P., You, L., Wu, X.Y., Sun, Y., 2011. Classification of cell types using a microfluidic device for mechanical and electrical measurement on single cells. Lab Chip 11 (18), 3174–3181.

Donadello, K., Piagnerelli, M., Reggiori, G., Gottin, L., Scolletta, S., Occhipinti, G., Zouaoui Boudjeltia, K., Vincent, J.L., 2015. Reduced red blood cell deformability over time is associated with a poor outcome in septic patients. Microvasc. Res. 101, 8–14.

Dylan Tsai, C.-H., Sakuma, S., Arai, F., Taniguchi, T., Ohtani, T., Sakata, Y., Kaneko, M., 2014. Geometrical alignment for improving cell evaluation in a microchannel with application on multiple myeloma red blood cells. RSC Adv. 4 (85), 45050–45058.

Ekpenyong, A.E., Toepfner, N., Fiddler, C., Herbig, M., Li, W., Cojoc, G., Summers, C., Guck, J., Chilvers, E.R., 2017. Mechanical deformation induces depolarization of neutrophils. Sci. Adv. 3 (6), e1602536.

Gabriele, S., Benoliel, A.M., Bongrand, P., Theodoly, O., 2009. Microfluidic investigation reveals distinct roles for actin cytoskeleton and myosin II activity in capillary leukocyte trafficking. Biophys. J. 96 (10), 4308–4318.

Gawad, S., Schild, L., Renaud, P.H., 2001. Micromachined impedance spectroscopy flow cytometer for cell analysis and particle sizing. Lab Chip 1 (1), 76–82.

Gossett, D.R., Tse, H.T., Lee, S.A., Ying, Y., Lindgren, A.G., Yang, O.O., Rao, J., Clark, A.T., Di Carlo, D., 2012. Hydrodynamic stretching of single cells for large population mechanical phenotyping. Proc. Natl. Acad. Sci. USA 109 (20), 7630–7635.

Guo, Q., Reiling, S.J., Rohrbach, P., Ma, H., 2012. Microfluidic biomechanical assay for red blood cells parasitized by Plasmodium falciparum. Lab Chip 12 (6), 1143–1150.

Haase, K., Pelling, A.E., 2015. Investigating cell mechanics with atomic force microscopy. J. R. Soc. Interface 12 (104), 20140970.

Herling, T.W., Müller, T., Rajah, L., Skepper, J.N., Vendruscolo, M., Knowles, T.P.J., 2013. Integration and characterization of solid wall electrodes in microfluidic devices fabricated in a single photolithography step. Appl. Phys. Lett. 102 (18), 184102.

Hochmuth, R.M., 2000. Micropipette aspiration of living cells. J. Biomech. 33 (1), 15–22.

Hou, H.W., Li, Q., Lee, G., Kumar, A., Ong, C., Lim, C.T., 2009. Deformability study of breast cancer cells using microfluidics. Biomed. Microdevices 11 (3), 557–564.

Hou, H.W., Warkiani, M.E., Khoo, B.L., Li, Z.R., Soo, R.A., Tan, D.S.-W., Lim, W.-T., Han, J., Bhagat, A.A.S., Lim, C.T., 2013. Isolation and retrieval of circulating tumor cells using centrifugal forces. Sci. Rep. 3, 1259.

Huang, L., Zhao, P., Wang, W., 2018. 3D cell electrorotation and imaging for measuring multiple cellular biophysical properties. Lab Chip 18 (16), 2359–2368.

Kim, J., Han, S., Lei, A., Miyano, M., Bloom, J., Srivastava, V., Stampfer, M.R., Gartner, Z.J., LaBarge, M.A., Sohn, L.L., 2018. Characterizing cellular mechanical phenotypes with mechano-node-pore sensing. Microsyst. Nanoeng. 4, 17091.

Ma, Z., Teo, A., Tan, S., Ai, Y., Nguyen, N.-T., 2016. Self-aligned interdigitated transducers for acoustofluidics. Micromachines 7 (12), 216.

Mak, M., Erickson, D., 2013. A serial micropipette microfluidic device with applications to cancer cell repeated deformation studies. Integr. Biol. 5 (11), 1374–1384.

Mazur, M.T., 1977. Macrophage deformability and phagocytosis. J. Cell Biol. 75 (1), 185–199.

Pedregosa, F., Varoquaux, G., Gramfort, A., Michel, V., Thirion, B., Grisel, O., Blondel, M., Prettenhofer, P., Weiss, R., Dubourg, V., 2011. Scikit-learn: machine learning in Python. J. Mach. Learn. Res. 12, 2825–2830.

Petchakup, C., Tay, H.M., Yeap, W.H., Dalan, R., Wong, S.C., Li, K.H.H., Hou, H.W., 2018. Label-free leukocyte sorting and impedance-based profiling for diabetes testing. Biosens. Bioelectron. 118, 195–203.

Puttaswamy, S.V., Xue, P., Kang, Y., Ai, Y., 2015. Simple and low cost integration of highly conductive three-dimensional electrodes in microfluidic devices. Biomed. Microdevices 17 (1), 4.

Rashid, T., 2016. Make Your Own Neural Network. CreateSpace Independent Publishing Platform.

Ren, X., Ghassemi, P., Kanaan, Y.M., Naab, T., Copeland, R.L., Dewitty, R.L., Kim, I., Strobl, J.S., Agah, M., 2018. Kernel-based microfluidic constriction assay for tumor sample identification. ACS Sens. 3 (8), 1510–1521.

So, J.H., Dickey, M.D., 2011. Inherently aligned microfluidic electrodes composed of liquid metal. Lab Chip 11 (5), 905–911.

Teng, Y., Pang, M., Huang, J., Xiong, C., 2017. Mechanical characterization of cancer cells during TGF-β1-induced epithelial-mesenchymal transition using an electrodeformation-based microchip. Sens. Actuators B Chem. 240, 158–167.

Teng, Y., Zhu, K., Xiong, C., Huang, J., 2018. Electrodeformation-based biomechanical chip for quantifying global viscoelasticity of cancer cells regulated by cell cycle. Anal. Chem. 90 (14), 8370–8378.

Wirtz, D., Konstantopoulos, K., Searson, P.C., 2011. The physics of cancer: the role of physical interactions and mechanical forces in metastasis. Nat. Rev. Cancer 11 (7), 512.

Wu, P.H., Aroush, D.R., Asnacios, A., Chen, W.C., Dokukin, M.E., Doss, B.L., Durand-Smet, P., Ekpenyong, A., Guck, J., Guz, N.V., Janmey, P.A., Lee, J.S.H., Moore, N.M., Ott, A., Poh, Y.C., Ros, R., Sander, M., Sokolov, I., Staunton, J.R., Wang, N., Whyte, G., Wirtz, D., 2018. A comparison of methods to assess cell mechanical properties. Nat. Methods 15, 491–498.

Yang, X., Chen, Z., Miao, J., Cui, L., Guan, W., 2017. High-throughput and label-free parasitemia quantification and stage differentiation for malaria-infected red blood cells. Biosens. Bioelectron. 98, 408–414.

Zhao, Y., Chen, D., Luo, Y., Li, H., Deng, B., Huang, S.B., Chiu, T.K., Wu, M.H., Long, R., Hu, H., Zhao, X., Yue, W., Wang, J., Chen, J., 2013. A microfluidic system for cell type classification based on cellular size-independent electrical properties. Lab Chip 13 (12), 2272–2277.

Zheng, Y., Shojaei-Baghini, E., Azad, A., Wang, C., Sun, Y., 2012. High-throughput biophysical measurement of human red blood cells. Lab Chip 12 (14), 2560–2567.

Zhou, Y., Basu, S., Laue, E., Seshia, A.A., 2016a. Single cell studies of mouse embryonic stem cell (mESC) differentiation by electrical impedance measurements in a microfluidic device. Biosens. Bioelectron. 81, 249–258.

Zhou, Y., Basu, S., Laue, E.D., Seshia, A.A., 2016b. Dynamic monitoring of single cell lysis in an impedance-based microfluidic device. Biomed. Microdevices 18 (4), 56.

Zhou, Y., Yang, D., Zhou, Y., Khoo, B.L., Han, J., Ai, Y., 2018. Characterizing deformability and electrical impedance of cancer cells in a microfluidic device. Anal. Chem. 90 (1), 912–919.